Characterization of Particle Motion and Deposition Behaviour in Electro-Static Fields

G Boiger
ICP Institute of Computational Physics, School of Engineering, Zurich University of Applied Sciences, Switzerland

ABSTRACT
As a prerequisite for studying and ultimately improving the powder coating process, particle motion and deposition effects within flow- and electro-static fields need to be thoroughly understood and thus characterized. In this context, a range of dimensionless groups is proposed and new means of characterization are presented. Considering the impact of electro-static, fluid-dynamic and gravity forces on coating particle motion, a triangle chart notation to characterize the state of varying particle size classes, is introduced. Furthermore a derivation of the dimensionless particle momentum equation is shown to lead to a dimensionless chart, representing all possible process states of coating. In combination with a Eulerian-LaGrangian, numerical model [1], the new means of characterization have led to a far better, over all perspective of occurring phenomena and their causes. Some examples are demonstrated here.

1. INTRODUCTION

The quality of electro-static powder coating processes of metal substrates is related to the uniformity of coating layer thickness. To increase this uniformity, knowledge based adaptions of process parameters and or geometry of the set-up are needed.

In order to create the basis for such improvement efforts, a thorough understanding of particle motion and deposition effects within flow- and electro-static fields is required. In addition to previous research (see e.g.: [2], [3] and [4]), this work presents recent advances in terms of characterization and modelling [1] of the coating process.

1.1. Over View

Chapter 2 of this paper is dedicated to the characterization of governing effects concerning the relation of acting forces. Thus three dimensionless groups and a corresponding triangle chart notation, representing the interaction of acting particle forces, are worked out. Chapter 3 is about the introduction of the dimensionless chart of coating states. Thereby the dimensionless, governing particle momentum equation (PME), which is derived in chapter 3.1, is used to produce two additional, dimensionless numbers in chapter 3.2. These numbers are then applied to form the dimensions of a chart, capable of representing all possible states of coating for a given geometrical set up. The dimensionless chart of coating states is presented in chapter 3.3. In addition to that, the combination of numerical modelling and dimensionless

*Corresponding Author: gernot.boiger@zhaw.ch

charting is sought. Therefore chapter 3.3 also presents the results of a numerical Euler-LaGrangian coating model [1]. As the model is applied to representative example cases, the results give enough insight into the actual meaning behind the distinct, dimensionless parameter combinations, to be able to roughly structure the coating chart into zones of force dominance.

1.2. Basics of the Powder Coating Process

The powder coating process is basically about a coating pistol, equipped with a negatively charged high voltage electrode, a grounded metallic substrate and e.g. thermoplastic or thermoset polymer coating particles with diameters: $5\mu m < D_p < 300\mu m$ [3]. The particles are carried by an air- flow through the pistol, past the electrode and into the coating chamber towards the substrate.

Close to the negatively charged electrode, oxygen ionization processes cause the presence of spatial charges of free electrons e^-, positively charged oxygen ions O^+_2 and negatively charged oxygen ions O^-_2 [5]. Figure 1 gives an impression of typical charge carrier densities n (cm^{-3}) as a function of distance r (cm) to the electrode. From Figure 1 it becomes clear that, for $r > 10^{-3}$m, negatively charged oxygen ions are the main carriers of spatial charges. In effect it is mainly the negatively charged oxygen ions that attach themselves to the surface of the passing coating particles.

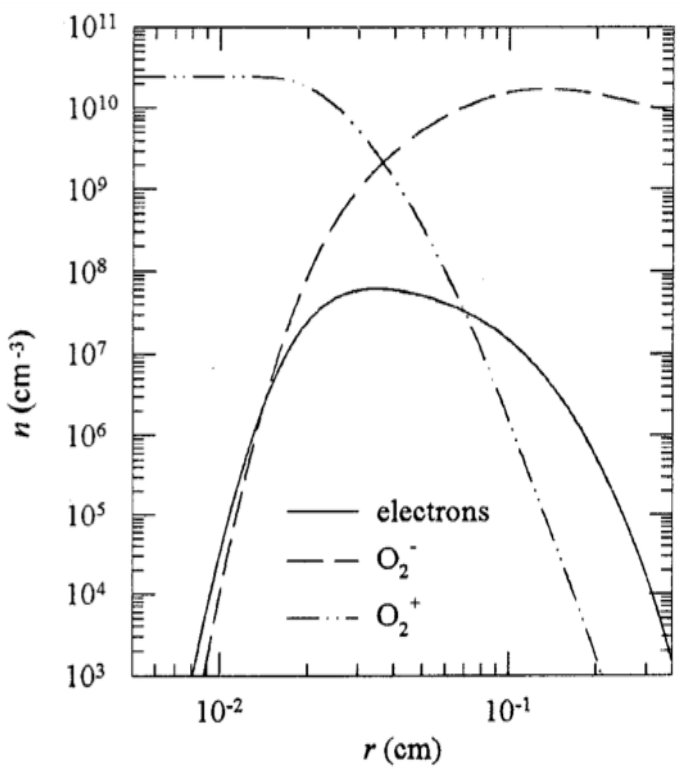

Figure 1: Charge carrier densities n (cm^{-3}) as a function of distance r to the electrode, [5].

As the coating particles are charged up to a negative surface specific charge q_p (C/m^2), they get impacted by the spatial electric field $\vec{E}$(x,y,z) (N/C). Upon entering the space between the charging zone and the substrate (the coating chamber), three main sorts of acting forces determine particle motion and particle-substrate deposition behaviour: gravity forces $\vec{F}_g$, electric forces $\vec{F}_{el}$ and fluid- drag forces $\vec{F}_f$, [1].

2. CHARACTERIZATION OF GOVERNING EFFECTS REGARDING FORCE RELATIONS

The equations for describing the three relevant, acting types of particle forces are well known and summed up in Table 1. Thereby spherical particles are assumed. Even though the flow situation within the coating chamber is expected to be turbulent, relative flow between air and particles is not. Thus a laminar particle–air drag relation can be used. In Table 1, D_p (m) is the particle-diameter, ρ_p and ρ_a (kg/m3) are the particle- and air densities respectively, μ_a (Pas) is the dynamic viscosity of air and $\vec{v}_{p,a}$ (m/s) is the relative flow velocity between particles and air.

Table 1: Relations for acting particle forces.

Name	**Unit**	**Relation**
Gravity /Buoyancy Force	N	$\vec{F}_g = \frac{\pi}{6}\left(\rho_p - \rho_a\right) D_p^3 \vec{g}$
Fluid Drag Force	N	$\vec{F}_f = 8\pi\mu_a D_p \vec{v}_{p,a}$
Electric Force	N	$\vec{F}_{el} = \pi q_p D_p^2 \vec{E}$
Drag of Sphere in Laminar Flow	-	$c_d = 64 / \mathrm{Re}_p$
Particle Reynolds Number	-	$\mathrm{Re}_p = \frac{\left\|\vec{v}_{p,a}\right\| D_p \rho_p}{\mu_a}$

2.1. Force Relations

As seen in Table 1, all three types of acting forces depend on the particle diameter with varying proportionality, such that: $\vec{F}_g = f(D_p^3)$, $\vec{F}_{el} = f(D_p^2)$ and $\vec{F}_f = f(D_p)$. A simple evaluation of these dependencies, for an exemplary case (Figure 2, bottom) shows that for small particles (e.g.: case Figure 2, D_p < 20µm) fluid drag forces dominate; that for medium sized particles (e.g.: case Figure 2, 20µm < D_p < 230µm) electric forces dominate; and that large particle motion (e.g.: case Figure 2, D_p > 230µm) is dominated by gravity. These initial insights do correspond with findings from practical applications, which report highest coating efficiencies for medium sized particles.

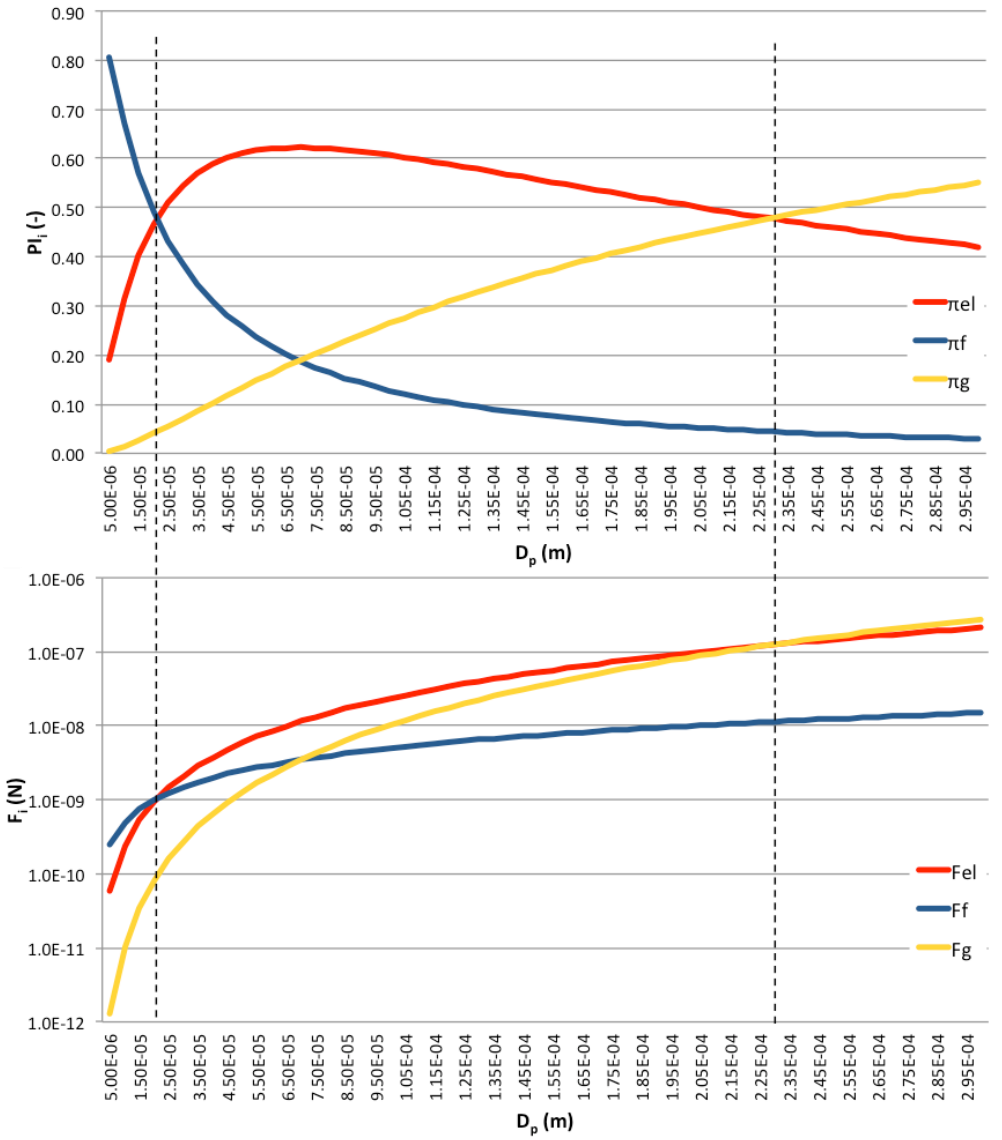

Figure 2: Exemplary case (ρ_P = 1300kg/m^3, q_P = 1C/m^2, max(vp,a) = 0.1m/s, max(E) = 0.75 N/C, μ_a = 1.98e-5 Pas) of maximum acting particle forces (bottom) and dimensionless force groups π_i (top) against particle diameter D_P. D_P < 20µm: dominance of fluid drag force; 20µm < D_P < 230µm: dominance of electric forces; D_P > 230µm: dominance of gravity force.

2.2. Dimensionless Groups to Characterize Force Relations

A new descriptive method to characterize the flow path and substrate-impact-position of each coating particle is hereby introduced. On the basis of relating the maximum, individual force contributions to the sum of all acting forces, the particle state can be completely characterized within the coating chamber. Thus three dimensionless groups π_f, π_{el} and π_g are obtained, which represent fluid drag, electric effects and gravity respectively. A fourth dimensionless group πm, representing the effects of inertia in relation to the acting forces, can be defined via the additional introduction of a characteristic length scale L_r (m) and a characteristic particle residence time τ_r (s). However, it turns out that πm is directly proportional to πg, which means that it is redundant information when characterizing the particle flow path. The definitions of π_f, π_{el}, π_g and π_m are found in Table 2.

Table 2: Signs, definitions and corresponding relations to particle - and process parameters of dimensionless force-relation groups.

Sign	Definition	Relation to Particle-/Process Parameters
π_f	$\frac{\left\|\max\left(\vec{F}_f\right)\right\|}{\left\|\max\left(\vec{F}_{el}\right)\right\|+\left\|\max\left(\vec{F}_g\right)\right\|+\left\|\max\left(\vec{F}_f\right)\right\|}$	$\frac{48\mu_a\left\|\max\left(\vec{v}_{p,a}\right)\right\|}{6q_pD_p*\left\|\max\left(\vec{E}\right)\right\|+\rho_pD_p^2*\left\|\vec{g}\right\|+48\mu_a\left\|\max\left(\vec{v}_{p,a}\right)\right\|}$
π_{el}	$\frac{\left\|\max\left(\vec{F}_{el}\right)\right\|}{\left\|\max\left(\vec{F}_{el}\right)\right\|+\left\|\max\left(\vec{F}_g\right)\right\|+\left\|\max\left(\vec{F}_f\right)\right\|}$	$\frac{6q_pD_p*\left\|\max\left(\vec{E}\right)\right\|}{6q_pD_p*\left\|\max\left(\vec{E}\right)\right\|+\rho_pD_p^2*\left\|\vec{g}\right\|+48\mu_a\left\|\max\left(\vec{v}_{p,a}\right)\right\|}$
π_g	$\frac{\left\|\max\left(\vec{F}_g\right)\right\|}{\left\|\max\left(\vec{F}_{el}\right)\right\|+\left\|\max\left(\vec{F}_g\right)\right\|+\left\|\max\left(\vec{F}_f\right)\right\|}$	$\frac{\rho_pD_p^2*\left\|\vec{g}\right\|}{6q_pD_p*\left\|\max\left(\vec{E}\right)\right\|+\rho_pD_p^2*\left\|\vec{g}\right\|+48\mu_a\left\|\max\left(\vec{v}_{p,a}\right)\right\|}$
π_m	$\pi_m=f\left(m_p,L_r,\tau_r,\sum_i\vec{F}_i\right)$	$\pi_m=\frac{m_pL_r}{\tau_r^2\sum_{i=3}\max\left(\left\|\vec{F}_i\right\|\right)}$
π_m	$\pi_m=f(\pi_g)$	$\pi_m=\frac{L_r}{\tau_r^2\left\|\vec{g}\right\|}\pi_g$

As a consequence of the definitions of π_f, π_{el} and π_g, Eqn.1 can be written as:

$$p_f+p_{el}+p_g=1 \tag{1}$$

Figure 2 shows a direct comparison between representing an exemplary case by inserting the dimensionless groups (top) and by using absolute values (bottom).

2.3. Triangle Chart Notation

Considering Eqn.1, as well as the definitions of π_f, π_{el} and π_g, a triangle chart notation is proposed here. By defining the three dimensionless groups as dimensions, the chart can be used to visually characterize the states of particle flow paths for any set of process parameters and any combination of particle properties. Since a coating particle cloud usually features poly-disperse particle size distributions, the state of one entire coating procedure cannot

simply be represented by one single dot in the triangle chart. Each particle size class will be placed at different locations within the chart, such that a non-linear, yet continuous, representative curve can be drawn to characterize the coating state of the entire cloud. Figure 3 shows a dimensionless triangle chart, with representative coating curves for three exemplary coating process parameter sets (Table 3). Note that for each case, smaller particles are located within the flow-dominated section, while larger particles tend to be found within the gravity section. Intermediate particle sizes can either be placed within the electro-statically dominated region, or at least have a tendency towards stronger electro-static impact.

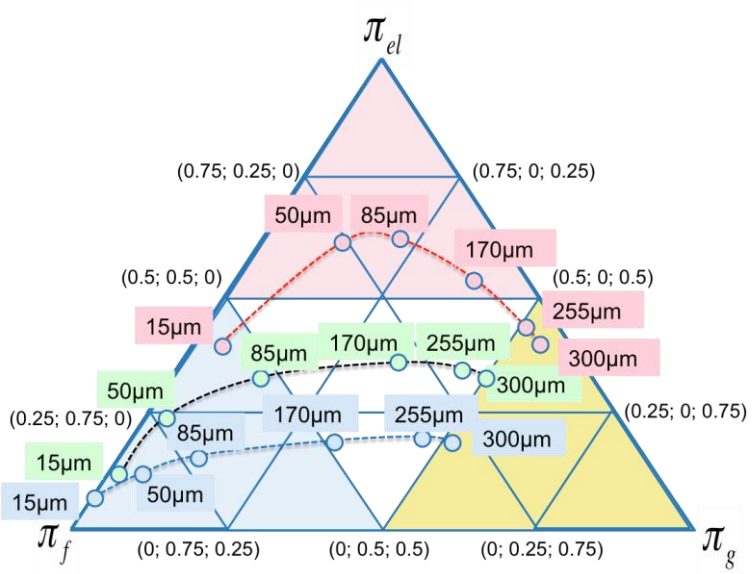

Figure 3: Dimensionless triangle chart of coating states. Electro-statically-, flow- and gravity dominated states are coloured in red, blue and yellow respectively. Three characteristic curves for three selected, exemplary coating states are shown. The respective process parameters of the electro- statically dominated (red curve), the flow dominated (blue curve) and the intermediate case (green curve), are shown in Table 3.

Table 3: Coating process parameter sets of three selected, exemplary cases, depicted in Figure 3.

Dominating Effect	**Coloration of Curve in Figure 3**	**Process Parameter Set**
Electric Forces	Red	$\left\|\max\left(\vec{E}\right)\right\| = 0.75N/C; q_p = 1C/m^2;$
		$\left\|\max\left(\vec{v}_{p,a}\right)\right\| = 0.1m/s$
Fluid Drag Forces	Blue	$\left\|\max\left(\vec{E}\right)\right\| = 0.40N/C; q_p = 1C/m^2;$
		$\left\|\max\left(\vec{v}_{p,a}\right)\right\| = 1.0m/s$
Intermediate	Green	$\left\|\max\left(\vec{E}\right)\right\| = 0.65N/C; q_p = 1C/m^2;$
		$\left\|\max\left(\vec{v}_{p,a}\right)\right\| = 0.6m/s$

3. PARTICLE MOMENTUM EQUATION AND CHART OF COATING STATES

In addition to the force-relation-characterization method, presented in chapter 2, another characterization method, based on the dimensionless particle momentum equation (PME), has been developed. It amounts to the dimensionless chart of coating states and is presented in the following.

3.1. Dimensionless Particle Momentum Equation

Assuming LaGrangian particle perspective, Newton's second law, in combination with the acting force relations, shown in Table 1, gives the governing PME for coating processes, as seen in Eqn. 2. Thereby $\ddot{\vec{x}}_p$ is particle acceleration and mp the particle mass.

$$m_p \frac{d^2 \vec{x}_p}{dt^2} = 8\pi\mu_a D_p \vec{v}_{a,p} + \frac{\pi}{6}\left(\rho_p - \rho_a\right) D_p^3 \vec{g} + \pi q_p D_p^2 \vec{E} \tag{2}$$

Combining the relations, seen in Table 4, with Eqn.2, the dimensionless version of the governing PME has been derived. It is depicted in Eqn.3. In Table 4 the sign '*' signifies the non-dimensionality of a variable, v_p (m/s) is the particle velocity, max(v_p) (m/s), max(v_a) (m/s), max($v_{a,p}$) (m/s) and max(E) (N/C) are the characteristic maximum particle velocity, air-flow velocity, relative air-particle velocity and maximum electric field strength respectively. Being the smallest extension of any numerical mesh cell, Δx has been brought into the considerations to create a link to related, numerical modelling efforts [1].

Table 4: Relations for the derivation of the dimensionless PME (Eqn. 3) out of Eqn. 2.

Description	**Relation**
(Dimensionless) Particle Velocity	$\vec{v}_p = \left\lvert \max\left(\vec{v}_p\right) \right\rvert * \vec{v}_p^*$
(Dimensionless) Time	$t = \frac{\Delta x}{\left\lvert \max\left(\vec{v}_p\right) \right\rvert} * t^*$
(Dimensionless) Particle Acceleration	$\frac{d^2 \vec{x}_p}{dt^2} = \frac{d\vec{v}_p}{dt} = \frac{\left\lvert \max\left(\vec{v}_p\right) \right\rvert^2}{\Delta x} * \frac{d\vec{v}_p^*}{dt^*}$
Maximum Particle Velocity	$\left\lvert \max\left(\vec{v}_p\right) \right\rvert = \frac{q_p D_p}{8\mu_a} * \left\lvert \max\left(\vec{E}_{\max}\right) \right\rvert + \left\lvert \max\left(\vec{v}_a\right) \right\rvert$
Maximum Air-Particle Relative Velocity	$\left\lvert \max\left(\vec{v}_{a,p}\right) \right\rvert = \frac{q_p D_p}{8\mu_a} * \left\lvert \max\left(\vec{E}_{\max}\right) \right\rvert$

Note that the relation for calculating maximum particle velocity in Table 4 is chosen, such that the co-located occurrence of extreme states within the flow- and the electric field is assumed. The relation for relative maximum air-particle velocity in Table 4 considers a state of equilibrium between viscose fluid drag and electro-static forces. It shows that high relative

fluid-particle velocities can only be achieved in regions of high electric field strength.

$$\frac{d^2\vec{x}_p^*}{dt^{*2}} = \frac{8\pi\mu_a D_p}{m_p} * \frac{\left|\max(\vec{v}_{a,p})\right|\Delta x}{\left|\max(\vec{v}_p)\right|} * \vec{v}_{p,a}^* + \frac{\rho_p - \rho_a}{\rho_p} * \frac{\Delta x}{\left|\max(\vec{v}_p)\right|^2} * \vec{g} + \frac{6q_p}{\rho_p D_p} * \frac{\left|\max(\vec{E})\right|\Delta x}{\left|\max(\vec{v}_p)\right|^2} * \vec{E}^* \tag{3}$$

3.2. Dimensionless Groups to Characterize the Coating State

Combining Eqn. 3 with the relations for the maximum air- particle- and particle velocity, seen in Table 4, two decisive dimensionless groups can be derived. The first, $\pi_{el/g}$ depicting the relation between electro- static and gravity effects (Eqn. 4) and the second $\pi_{f/el,i}$ relating fluid viscose drag to electro-static times inertial effects (Eqn.5).

$$\pi_{el/g} = \frac{6q_p\left|\max(\vec{E})\right|}{(\rho_p - \rho_a)D_p\left|\vec{g}\right|} \tag{4}$$

$$\pi_{f/el,i} = \frac{384\mu_a^2 q_p\left|\max(\vec{E})\right|\Delta x}{\rho_p D_p * \left(q_p D_p\left|\max(\vec{E})\right| + 8\mu_a\left|\max(\vec{v}_a)\right|\right)^2} \tag{5}$$

In the context of creating a suitable, LaGrangian particle model of the coating process, another dimensionless number πt to represent the relation between numerical particle-time step Δt and particle relaxation time τp is proposed according Eqn.6, [6].

$$\rho_t = \frac{\mathrm{D}t}{t_p} = \frac{48\eta_a \mathrm{D}t}{r_p D_p^2} \tag{6}$$

While $\pi_{el/g}$ and $\pi_{f/el,i}$ reflect the physical state of the coating process, π_t reflects the quality of the numerical time step and should be kept well below 1 at all times. Choosing π_t too high will result in an un-physical, merely numerical alteration of calculated particle paths.

3.3. Dimensionless Chart of Coating States

The dimensionless groups $\pi_{el/g}$ and $\pi_{f/el,i}$ span a two-dimensional space which encompasses all possible coating states for all possible combinations of particle- and process parameters. This two dimensional space constitutes the coating chart, shown in Figure 4.

By combining the coating chart characterization methodology with results form numerical simulations [1], we were able to interpret the coating chart and its zones in terms of applicable, practical meaning. Several numerical experiments at varying parameter configurations were conducted, the dimensionless numbers $\pi_{el/g}$ and $\pi_{f/el,I}$ of these cases were determined and the results were qualitatively checked. Thereby the evaluation criteria were: the shape of the coating particle cloud as well as the distribution of particle deposition patterns on the front- and back-side of a metallic plate. On the basis of these evaluations, a qualitative distinction between chart-zones of varying force-dominance could be made. Of course it is impossible to part the individual zones by calculated curves, since transitions are blurred and strongly

related to the observed effects. Thus the achieved structure in Figure 4 is relatively rough and leaves room for interpretation. Still it does constitute a first design guideline for practical application.

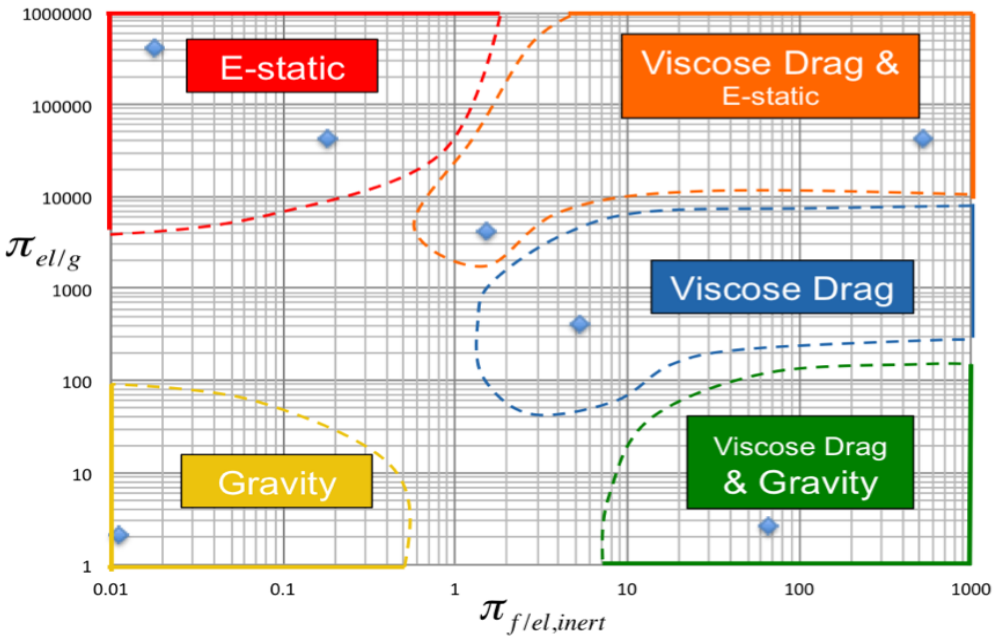

Figure 4: Qualitatively structured chart of two-dimensional space of all possible states of the powder coating process. Dominating effects within chart zones are shown as derived from numerical modelling [1]: electro-static (red), gravity (yellow), flow (blue), combination of flow & electro-static (orange) and combination of flow & gravity (green). The dashed confines are qualitative in nature.

4. CONCLUSION

Being the basis of thoroughly understanding the coating process, new means of proper characterization have been worked out and presented. While the proposed triangle chart notation (chapter 2) helps to understand the acting force relations on individual particles, the chart of coating states (chapter 3) provides a more practically applicable view on the entire process. Where the triangle chart notation concentrates on individual particles, the chart of coating states focuses on the big picture. Both characterization methods have already been applied in combination with a new numerical, OpenFoam® [7] based solver. The corresponding results have on the one hand led to interpreting the coating chart (Figure 4) and have on the other hand already greatly contributed to achieving a much better understanding of cause-effect relations for the coating process as a whole. These findings are published in [1].

This work will thus constitute the foundation of future, knowledge based improvement efforts in terms of optimized coating process parameter combinations.

REFERENCES

[1] G. Boiger, (2016). Eulerian-LaGrangian model of particle laden flows and deposition effects in electro-static fields based on OpenFoam, Int. Journal of Multiphysics; Vol. 10 (2), pp. 177-194.

[2] K. Pulli, (2006). Optimierung der Pulverlackapplikation durch Anwendung experimenteller und numerischer Untersuchungsverfahren. PhD thesis. University of Stuttgart, Stuttgart, Germany, ISBN: 3-936947-96-1, URN: ngn:de:bsz:93-opus-28054, 2006.

[3] A.G. Bailey, (1998). The science and technology of electrostatic powder spraying, transport and coating, University of Southampton, Southampton, UK, Journal of Electrostatics; Vol.45, (1998), pp. 85-120;

[4] P. Plascar, (2003). Untersuchungen zur Wechselwirkung zwischen Strömungsmechanik und Elektrostatik bei der Neuentwicklung von Flachstrahldüsen zur Verbesserung des Auftragswirkungsgrades im Pulverbeschichtungsprozess. Diploma thesis. Fachhochschule Esslingen a.N. Hochschule für Technik, Esslingen, Germany, 2003;

[5] F. Pontiga, C. Soria, A. Castellanos, (1996). Spatial Distribution of Electrons and Ions in a Negative Corona Discharge, Facultad de Fisica, E.U.A.T., Sevilla, Spain, Conference on Electrical Insulation and Dielectric Phenomena 1996, San Francisco, October 20-23; 0-7083-3580-5, 1996, IEEE Annual Report.

[6] G. Boiger, M. Mataln, W. Brandstätter, (2009). Adaptive time stepping for explicit Euler implementation of spherical and non-spherical particle speed up. ICE Stroemungsforschung GmbH., Montanuniversitaet Leoben. Int.Journal of Multiphysics; Vol.3, No.3, August 2009, pp. 267–291(25);

[7] H. G. Weller, G. Tabor, H. Jasak, C. Fureby, A tensorial approach to computational continuum mechanics using object-oriented techniques, Computers in Physics, Vol. 12, No. 6, Nov/Dec 1998.